JMEPEG (2024) 33:4647–4658
https://doi.org/10.1007/s11665-023-08272-y

1059-9495/$19.00

TECHNICAL ARTICLE

Influence of Samarium Oxide Addition on Magnesium Aluminate Spinel: A Case of Reaction Sintering

Biswajit Baruah and Ritwik Sarkar

Submitted: 2 March 2023 / Revised: 24 April 2023 / Accepted: 26 April 2023 / Published online: 9 May 2023

In the present study, the role of samarium oxide (Sm_2O_3) as an additive on the property development of stoichiometric (molar ratio MgO: Al_2O_3 = 1:1) magnesium aluminate spinel using different raw material sources was investigated. Initially, a total of 6 spinel batches were prepared with the help of commercially available sources of alumina (three different grades) and magnesia (two different grades) and then, the effect of Sm_2O_3 addition (1-4% by weight) on the properties of different spinel compositions was studied in the temperature range of 1550-1650 °C. The various spinel batches, both additive-free and Sm_2O_3 doped, were then characterized via densification, phase formation, microstructural studies, cold strength and retainment of strength post thermal shock. The results revealed that 1% of Sm_2O_3 addition led to optimum densification of all the spinel batches. This was due to the formation of samarium aluminate-$SmAlO_3$ formed as a result of reaction between Sm_2O_3 and components of spinel providing hindrance to the migration of grain-boundaries of spinel. An improvement in the cold-strength and retained strength post-thermal shock treatment in the Sm_2O_3-doped spinel compositions was also observed.

Keywords grain-growth restriction, magnesium aluminate spinel, reaction sintering, samarium aluminate, samarium oxide

1. Introduction

Magnesium aluminate ($MgAl_2O_4$) of Mag-Al spinel ceramics have become popular in various industries owing to their interesting combination of properties such as high strength and hardness at room as well as elevated temperatures, excellent corrosion resistance, and high thermal spalling resistance. (Ref 1, 2). Moreover, traditional refractories have been successfully replaced by $MgAl_2O_3$ spinel in high-temperature applications owing to their high thermal stability (melting point ~ 2135 °C) and high chemical resistance which are common in service conditions (Ref 3).

The myriad benefits of mag-al spinel are outweighed by its high processing cost and low sinterability, which makes it difficult to sinter (Ref 4-7). Researchers in the fields of ceramics and materials science have proposed a number of different methods for manufacturing Mag-Al spinel ceramics (Ref 8-14). These methods are promising in theory, but in practice they are limited to the laboratory because of their high cost and complicated operations. Due to its low production costs and commercial practicality, the solid-state reaction technique has been discussed in a number of papers (Ref 15-18). Spinel with enhanced densification and mechanical properties can be achieved using a two-step sintering process, but this method is impractical for mass production because of its high cost and long processing time (Ref 19). Evidence from previous research suggests that dense spinel products can be produced using a single-stage firing technique, which has clear commercial advantages over a two-stage firing process (Ref 20-22).

Numerous studies (Ref 23-37) have examined the effects of various additives on spinel properties, especially alkali/alkaline earth or transition metal compounds as SnO_2, ZrO_2, TiO_2, Cr_2O_3, ZnO, Cr_2O_3, AlF_3, Na_3AlF_6, $AlCl_3$, CaF_2, etc. However, rare-earth oxides (REOs) could be useful components in the production of spinel refractories as well due to their excellent thermal and chemical stability (Ref 38). An earlier study (Ref 39) summarized the role of various REOs on the sintering and property development of Mag-Al spinel.

Samaria (Sm_2O_3)-doped spinel products with improved density and strength using an *in situ* conventional mixing route were reported that Ma et al. (Ref 40), and this improvement in properties was attributed to the *in situ* formation of $SmAlO_3$ phase which was reported to be distributed in the intergranular space of spinel grains and restricted the grain growth (Ref 40). Another recent work (Ref 41) also showed that Sm_2O_3 doped in MgO-rich spinel also leads to improved density, microhardness and cold crushing strength due to the formation of rare-earth aluminate-$SmAlO_3$. It was further reported that although the presence of MgO phase affects the strength values, but those present in spinel grain boundaries engender a pinning effect and improves the sinterability of spinel (Ref 41). Dense spinel-based bodies with improved density, cold strength and resistance to thermal shock treatment were obtained by co-doping of Sm_2O_3 and La_2O_3 (15 wt.% with weight ratio of Sm_2O_3 and La_2O_3 = 1:1) in spinel obtained from commercial-grade sources of Al_2O_3 and MgO using a single-stage firing technique at 1680 °C for 4 h (Ref 15). $Sm_{4.67}(SiO_4)_3O$ and $La_{4.67}(SiO_4)_3O$ with rod-like morphology and $SmAlO_3$ and $La_{10}Al_4O_{21}$ microcrystalline phases with granular morphology were found in the doped

Biswajit Baruah and **Ritwik Sarkar**, Department of Ceramic Engineering, National Institute of Technology Rourkela, Odisha 769008, India. Contact e-mail: biswajit.baruah1991@gmail.com.

compositions which effectively prevented grain growth and led to improvement in properties (Ref 15). Ren and group (Ref 3) investigated and reported on the role of double-doping of REOs, i.e., Sm_2O_3 and (Y_2O_3, Nb_2O_5, and La_2O_3) on the property development of Mag-Al spinel with stoichiometric chemistries prepared from calcined MgO and Al_2O_3 using a single-stage firing process at 1580 °C for 4 h. Double-doping of REOs greatly improved the density, strength and thermal shock resistance of stoichiometric spinel and Sm_2O_3-Nb_2O_5 showed the maximum improvement. YAG (tetragonal) and $SmNbO_4$ (monoclinic), formed by Sm_2O_3-Y_2O_3 and Sm_2O_3-Nb_2O_5 additions, respectively, have a closely similar crystal structure to the spinel (cubic) formed resulting in increased densification and improved properties. However, the improvement in densities and other properties of Sm_2O_3-La_2O_3-doped compositions was attributed to the formation of rod-like morphologies due to the formation of phases such as $SmAlO_3$ and $MgAl_{11}LaO_{19}$, despite both of them having a hexagonal crystal structure (Ref 3).

Even though the preceding studies have evidenced the beneficial role of Sm_2O_3 addition on the sintering and characteristics of spinel, there is still a growing demand for future research in this area due to the limited number of reported works. Furthermore, only a handful of the reported studies have conformed to the methodical addition of Sm_2O_3. The adoption of an intermediary milling process prior to sintering is another noteworthy feature in the aforementioned studies. Although including an additional energy-intensive milling operation may improve the properties of the resulting spinel product, the overall cost of spinel production may increase further and make commercialization difficult. Although rare-earth oxides (REOs) are costly, the expenses on development of REO-doped spinel may be lowered by the use of commercial-grade raw materials along with a single-step conventional solid-state process that produces *in situ* spinel (as opposed to the more expensive pre-reacted spinel). Furthermore, the cost of these materials may be drastically reduced if the amount of REO additive used could be kept to a minimum.

An earlier study demonstrated the role of Y_2O_3 as a beneficial additive on the properties of Mag-Al spinel (Ref 42). This paper investigates the effect of adding varying amounts of Sm_2O_3, from 1 to 4 wt.%, to batches of stoichiometric Mag-Al spinel prepared by single-stage sintering from the same set of commercial-grade oxide reactants, without any intermediate milling procedure. Effect of Sm_2O_3 addition on spinel's density, phase formation, microstructure, and mechanical characteristics (cold strength, thermal shock behavior) was studied.

2. Experimental

Commercial grade reactants—3 sources of alumina (alumina-A, C and R; all from Almatis, India) and 2 sources of magnesia (MgO-light from Himedia Labs, India and fused MgO from a Chinese source), were used as the starting raw materials. Initially, a total of 6 MgO-Al_2O_3 based powder compositions, with molar ratio of MgO: Al_2O_3 = 1:1, were prepared, and then, the effect of systematic addition of Sm_2O_3 (1-4 wt.%) on these compositions was studied. The properties of raw materials and Sm_2O_3 are shown in Table 1. For the without-additive batches, two sources of raw materials (one of alumina and other of magnesia) were mixed in alcohol medium (2-propanol) and the contents were continuously stirred for 30 min via magnetic mixer (Tarsons, India) to ensure proper powder blending. The contents were then allowed to dry in an air oven (T_{oven} = 80 °C) following which 6 without-additive batches were obtained. Thereafter, each batch was divided into 5 equal halves, with 1 portion set aside for the additive-free (0 wt.%) batch and the other 4 were retained for the Sm_2O_3-doped batches. The remaining 4 parts were mixed with alcohol and 1, 2, 3, and 4 wt.% Sm_2O_3 (Lobachemie, India) for 30 min before being dried in an oven. After drying, each batch was combined with polyvinyl alcohol (4 wt.%) binder solution (conc. = 5%), then sieved and shaped into pellets (15 mm in diameter) and bars (60 mm by 6 mm by 6 mm) using a pressing machine (Model 3887, Carver Inc., made in the US) and high chromium steel molds at a forming pressure of 150 MPa and a dwell period of 60 s. The green cylindrical bodies were then dried in an oven maintained at 110 °C to get rid of any remnant free moisture in the samples. The samples were then sintered at 1550, 1600, and 1650 oC with 2 h dwelling at the peak temperatures using a raising-hearth furnace (Bysakh, India).

The sintered products were then investigated for phase identification studies using x-ray diffraction (XRD) method with the help of an x-ray diffractometer (Ultima-IV, Rigaku, Japan; $\lambda_{Cu\text{-}K\alpha}$ = 1.540640 Å). Densification of the sintered bodies was studied by measuring the bulk densities and apparent porosities by vacuum method (Archimedes' principle), and the immersing medium used was water (ρ_{water} = 1 g/cc). Elements in the gold-coated fractographs were analyzed at selected locations using an EDS (Energy-dispersive analysis of x-ray) detection unit (Model 51-ADD0013, Oxford instruments, UK) attached to a scanning electron microscope (JEOL JSM- 6480 LV, Japan). The cold strength of the 1650 °C sintered bars was evaluated via three-point bending method using a universal testing machine (Model HK10S, Tinius Olsen, USA).

For thermal shock study, flexural bars sintered at 1650 °C were first exposed to several water quench (thermal shock) cycles (2, 4, 6, and 8 cycles), and then, a 3-point flexural strength test was performed to estimate the retained or residual strength. Pre-sintered bars were heated to 1000 °C for ten minutes before being cooled in water. This process was repeated for a total of 8 thermal shock cycles. Figure 1 is a flowchart depicting the experimental technique. It is worth mentioning that for each data point in the plots of the current study, the average value obtained from testing 5 individual samples for each batch is reported.

4Furthermore, thermal expansion studies of the optimized samaria containing batch and its comparable additive-free batch were performed using a dilatometer (Netzsch DL 402SE, Germany). For this, rectangular bars of dimensions 8 × 5× 5 mm^3 were carefully prepared and the edges were smoothened out using an abrasive sheet. The rectangular green samples were heated with a rate of 5 °C min^{-1}, and the operating temperature of the dilatometer was from room temperature to 1500 °C.

Due to large number of batches in the present study, Table 2 is provided showing separate batch codes for the different spinel batches made without additive (undoped) and those made with the addition of Sm_2O_3 for clarity.

3. Results and Discussion

3.1 Physico-Chemical Characteristics of Raw Materials and Sm_2O_3

The properties of the various commercial grades of alumina and magnesia used in the present study are given in Table 1. All

Table 1 Properties of raw materials

Constituents → Raw materials ↓	Al_2O_3, %	Na_2O, %	Fe_2O_3, %	SiO_2, %	CaO, %	MgO, %	Specific surface area, m^2/g	Average particle size, μm
Al_2O_3-A (A)	99.8	0.07	0.02	0.03	0.02	0.05	8.9	0.5
Al_2O_3-C (C)	99.7	0.1	0.03	0.03	0.03	…	3	2.5
Al_2O_3-R (R)	99.8	0.08	0.02	0.03	0.03	…	7.2	0.6
MgO light (L)	0.09	0.04	0.01	0.08	1.16	98.31	43.88	0.26
Fused MgO (F)	0.07	0.26	0.22	0.4	1.4	97.35	0.06	28

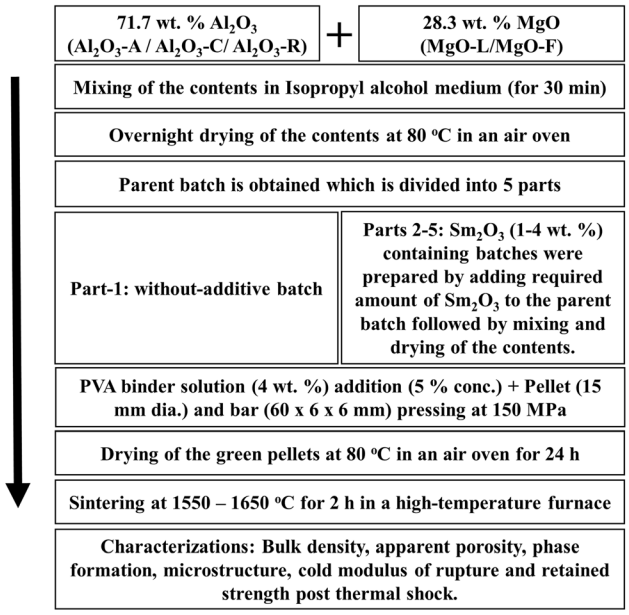

Fig. 1 Experimental procedure

the alumina fines used in this research were extremely pure (≥ 99.7%) and fine. Alumina-C ($d_{50} \sim 2.5\ \mu m$) was relatively coarser than the other two grades of alumina. So, in comparison with Alumina-C, Alumina-A and Alumina-R had a higher specific surface area. Between the grades of magnesia used, fused magnesia (MgO-F) was much coarser ($\sim 28\ \mu m$) than magnesia-light ($\sim 0.26\ \mu m$). So, the specific surface area of MgO-L ($\sim 43.88\ m^2/g$) was much higher than that of fused magnesia ($0.06\ m^2/g$). MgO light was relatively purer than fused magnesia with the latter having higher percentage of impurities (calcium oxide, silica, ferric oxide, and sodium oxide). High purity Sm_2O_3 (≥ 99.9%) with a molecular weight of 348.72 g/mol was used as additive.

3.2 Phase Identification

The detailed phase analysis study of the spinel batches using different raw material sources without samarium oxide was done in our previous work (Ref 42). Only magnesium aluminate spinel phase (ICDD file no. 01-070-5187) was obtained for the magnesia-light containing batches (AL, CL and RL) for all the sintering temperatures (1550, 1600 and 1650 °C), indicating the completion of spinel formation reaction. Whereas, spinel batches containing fused magnesia (AF, CF and RF) showed spinel phase (ICDD file no. 01-070-5187) as major one with little extent of periclase (MgO; ICDD file no. 00-045-0946) phase. As magnesia-light is considerably finer than fused magnesia, the former has a higher reactivity and enhanced the spinel formation reaction.

Phases such as spinel (ICDD file no. 01-073-2210), samarium aluminate ($SmAlO_3$; ICDD file no. 00-046-0394), and periclase (MgO; ICDD file no. 00-045-0946) were all identified in the 1 wt.% Sm_2O_3-doped spinel batches containing fused magnesia sintered at 1550 °C (Fig. 2a), while periclase was not present in the MgO-L based batches with 1 wt.% Sm_2O_3 sintered at the same temperature. This was presumably due to the large specific surface area (and hence higher reactivity) of magnesia light as compared to fused magnesia. Also, the 1 wt.% additive-containing spinel batches showed peaks of spinel and $SmAlO_3$ only at higher sintering temperatures 1600 (Fig. 2b) and 1650 °C (Fig. 2c). Higher sintering temperature facilitated greater reactions which likely explains why the peaks of spinel and $SmAlO_3$ phases were relatively stronger at these temperatures.

Sm_2O_3 reacts with Al_2O_3 and forms a samarium-rich secondary phase—$SmAlO_3$ which has a tetragonal crystal structure while the crystal structure of the parent spinel is cubic. In other words, the secondary phase has a crystal structure comparable to that of the formed spinel in each of the samaria-containing spinel batches formed at different firing temperatures. The distinct phases observed in the spinel batches, both additive free and 1-4 wt.% Sm_2O_3 containing ones, for all the sintering temperatures (1550-1650 °C) are listed in Table 3.

3.3 Density

The bulk densities (B.D.) of all the spinel batches, both additive-free and Sm_2O_3-doped types, sintered at different temperatures (1550, 1600 and 1650 °C) are shown in Fig. 3. At 1550 °C, the addition of 1 wt.% of Sm_2O_3 was found to favor the densification of spinel, while the addition of more amount of Sm_2O_3 (2-4 wt.%) led to reduction in density values (Fig. 3a). A similar trend in density changes was observed for the spinel batches sintered at 1600 °C and 1650 °C as shown in Fig. 3(b) and (c), respectively. For obvious reasons, due to enhanced diffusion and mass transfer with a rise in sintering temperature, the B.D. values of all the spinel batches (pristine as well as Sm_2O_3 doped) sintered at 1650 °C were greater than those fired at lower sintering temperatures (1550 and 1600 °C). Careful survey and inspection of Fig. 3 reveal that the spinel batches in our investigation acquired maximum densification upon coupling the effects of elevated temperature and a doping amount of 1 wt.% Sm_2O_3. Thus, 1 wt.% Sm_2O_3 was found to be the optimized level for densification in the current investigation.

For the pristine spinel batches, AF, CF and RF revealed higher B.D. values than their corresponding spinel batches associated with magnesia light—AL, CL and RL. The preced-

Table 2 Batch codes used for the additive-free and Sm_2O_3-doped spinel batches

Without-additive batches		Sm_2O_3-doped batches (where x = 1, 2, 3 or 4)	
Batch	**Batch codes**	**Batch**	**Batch codes**
Al_2O_3-A + MgO-L	AL	A + L + x % Sm_2O_3	AL-Sx
Al_2O_3-A + MgO-F	AF	A + F + x % Sm_2O_3	AF-Sx
Al_2O_3-C + MgO-L	CL	C + L + x % Sm_2O_3	CL-Sx
Al_2O_3-C + MgO-F	CF	C + F + x % Sm_2O_3	CF-Sx
Al_2O_3-R + MgO-L	RL	R + L + x % Sm_2O_3	RL-Sx
Al_2O_3-R + MgO-F	RF	R + F + x % Sm_2O_3	RF-Sx

ing phase identification study (Table 3.) already evidenced that at any given sintering temperature, the spinel batches with fused magnesia have remnants of periclase; while the spinel batches associated with magnesia light did not show any trace of unreacted MgO even at lower sintering temperature 1550 °C. Since specific surface area of MgO light and hence, its reactivity is more than that of fused magnesia, it stands to reason that the volumetric expansion in relation to the process of spinel formation is more in the spinel batches containing MgO-L which led to a fall in the measured bulk densities. Consequently, in the additive-free condition, the spinel batches having MgO-L showed a lower density value than those associated with MgO-F for all sintering temperatures. Further, spinel batches associated with Al_2O_3-C (batches CL and CF), in both additive-free and additive-containing conditions, had lower density values than their corresponding spinel batches associated with the other two grades of alumina (Al_2O_3-A and Al_2O_3-R). Among the three grades of alumina used, alumina-C had a relatively coarser particle size (Table 1.) which may have affected the process of sintering and hence, the density values for each temperature level.

Samarium aluminate ($SmAlO_3$) formed as a second phase is having a tetragonal crystal structure, which is in close similarity to the cubic crystal structure of the formed spinel, for all the sintering temperatures (Fig. 2), which may explain why adding 1 wt.% of Sm_2O_3 improved the density results. Similarity in crystal structure configuration has been known to aid in the process of densification by improving the mass transport mechanisms and assisting in pore shrinkage resulting in a matrix with controlled microstructure shrinkage (Ref 43, 44).

Additionally, it is also important to state that in all of the spinel batches doped with Sm_2O_3, some amount of alumina in the starting Al_2O_3-MgO-Sm_2O_3 mix was consumed at high temperature due to the formation of $SmAlO_3$ and the spinel formed in each case was not entirely stoichiometric, but a little excess in MgO. Since this extra MgO was so low in concentration, hence was not detectable in the x-ray diffraction experiments conducted at high sintering temperatures (1600 and 1650 °C). Oxygen vacancies occur at high temperatures in spinel compositions having a little surplus of MgO, which aids in the process of mass transfer and densification (Ref 22, 45). The defect reaction can be written as follows -

$$3MgO \xrightarrow{MgAl_2O_4} Mg_{Mg}^{x} + 2Mg'_{Al} + 3O_O^x + V_O^{\cdot\cdot} \qquad \text{(Eq 1)}$$

It is likely that the interaction between samarium oxide and alumina increased the quantity of secondary phase ($SmAlO_3$) formed when the Sm_2O_3 content was increased over 1 wt.%. As a consequence, the density of the formed *in situ* spinel may have been affected at higher amounts of Sm_2O_3 by the formation of a larger number of micropores in the local area (Ref 46).

In accordance with the phase diagram of Al_2O_3-ZrO_2-Sm_2O_3 system as reported by Lakiza and Lopato (Ref 47), the interaction between Sm_2O_3 and Al_2O_3 can lead to formation of compounds such as $SmAlO_3$ and $Sm_4Al_2O_9$ at 1250 and 1650 °C, respectively. However, in our current investigation, the phase studies at 1650 °C did not show any peak of $Sm_4Al_2O_9$ for any additive containing spinel batch. This was presumably due to the low amount of Sm_2O_3 additive used in the present study (maximum concentration = 4 wt.%). This observation is in agreement with the study carried out by Ma et al. (Ref 40) wherein Sm_2O_3 as high as 7.5 wt.% was used and yet no trace of $Sm_4Al_2O_9$ was found in the diffraction patterns.

3.4 Microstructure

Fractographs of spinel batches without any additive sintered at 1650 °C are depicted in Fig. 4. It appears that the microstructure of the batches of fused magnesia containing spinel batches (AF, CF, and RF) is more compact and denser than that of the batches having magnesia light (batches AL, CL and RL). According to the density studies, this is in line with what has been said thus far (Fig. 3c). Also, it seems that there are less pores in the spinel batches linked to fused magnesia than in the spinel batches containing MgO-L. It is further evident from Fig. 4. that the densification process was affected in the spinel batches containing finer magnesia light because the process of spinel formation (and hence volume expansion) was more extensive in these batches than that of fused magnesia containing batches.

Back-scattered images (fractographs) of spinel batches having 1 wt.% Sm_2O_3 and fired at 1650 °C are shown in Fig. 5. In comparison with equivalent additive-free spinel batches sintered at the same temperature (Fig. 4), the grain structure in these fractographs is more uniform. The formation of a samarium-rich secondary phase, samarium aluminate ($SmAlO_3$; tetragonal), with a comparable crystal structure to the *in situ* generated mag-al spinel (cubic), may account for the density increase. These $SmAlO_3$ phases (seen as white phases in the micrographs) seem to act as grain-growth barriers across the grain-boundaries of the produced spinel, thereby controlling the growth of spinel grains and aiding in stabilizing the spinel grain boundaries. This, in turn, might result in enhanced mechanical performance.

Fractographs (both undoped and 1 wt.% Sm_2O_3-doped spinel batches sintered at 1650 °C) along with their corre-

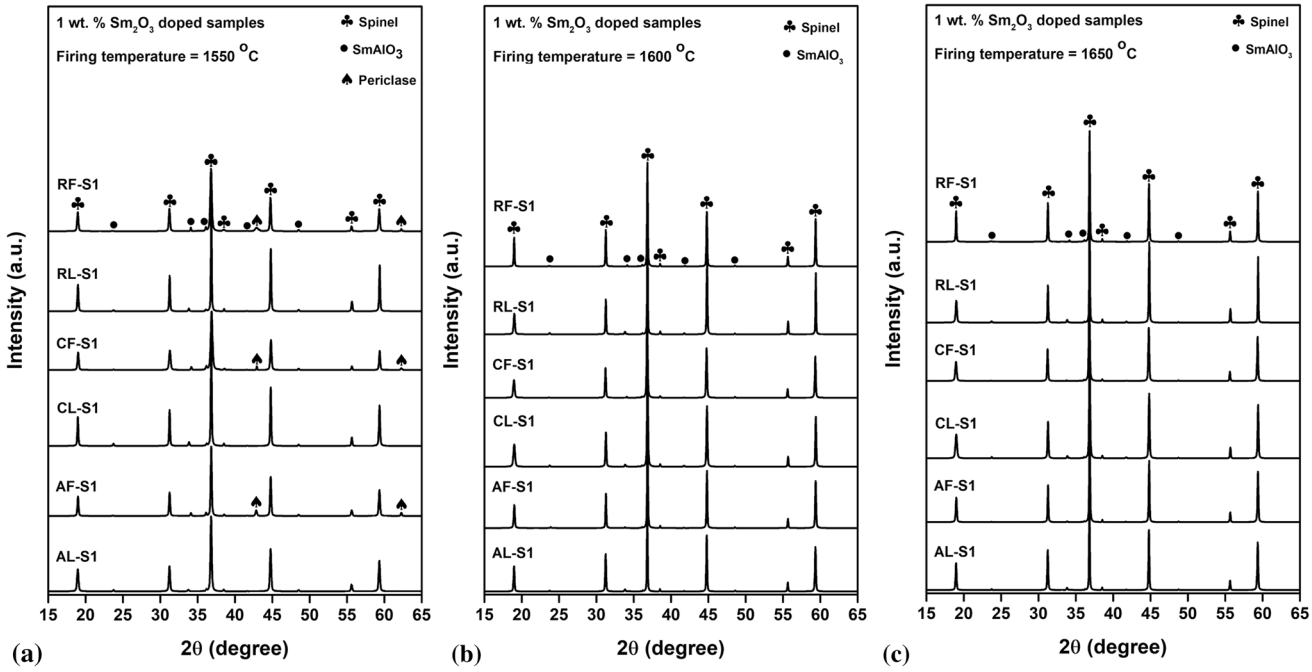

Fig. 2 Phase identification study of spinel batches doped with 1 wt.% Sm_2O_3 fired at (a) 1550 °C (b) 1600 °C (c) 1650 °C

Table 3 Phases obtained in the various spinel batches sintered at different temperatures

	Phases identified (Magnesium aluminate Spinel = S; Periclase = MgO; Samarium aluminate = $SmAlO_3$)		
Spinel batch	**1550, °C**	**1600, °C**	**1650, °C**
AL	S	S	S
AF	S, MgO	S, MgO	S, MgO
CL	S	S	S
CF	S, MgO	S, MgO	S, MgO
RL	S	S	S
RF	S, MgO	S, MgO	S, MgO
AL-S1	S, $SmAlO_3$	S, $SmAlO_3$	S, $SmAlO_3$
AF-S1	S, MgO and $SmAlO_3$	S, $SmAlO_3$	S, $SmAlO_3$
CL-S1	S, $SmAlO_3$	S, $SmAlO_3$	S, $SmAlO_3$
CF-S1	S, MgO and $SmAlO_3$	S, $SmAlO_3$	S, $SmAlO_3$
RL-S1	S, $SmAlO_3$	S, $SmAlO_3$	S, $SmAlO_3$
RF-S1	S, MgO and $SmAlO_3$	S, $SmAlO_3$	S, $SmAlO_3$
AL-S2	S, $SmAlO_3$	S, $SmAlO_3$	S, $SmAlO_3$
AF-S2	S, MgO and $SmAlO_3$	S, $SmAlO_3$	S, $SmAlO_3$
CL-S2	S, $SmAlO_3$	S, $SmAlO_3$	S, $SmAlO_3$
CF-S2	S, MgO and $SmAlO_3$	S, $SmAlO_3$	S, $SmAlO_3$
RL-S2	S, $SmAlO_3$	S, $SmAlO_3$	S, $SmAlO_3$
RF-S2	S, MgO and $SmAlO_3$	S, $SmAlO_3$	S, $SmAlO_3$
AL-S3	S, $SmAlO_3$	S, $SmAlO_3$	S, $SmAlO_3$
AF-S3	S, MgO and $SmAlO_3$	S, $SmAlO_3$	S, $SmAlO_3$
CL-S3	S, $SmAlO_3$	S, $SmAlO_3$	S, $SmAlO_3$
CF-S3	S, MgO and $SmAlO_3$	S, $SmAlO_3$	S, $SmAlO_3$
RL-S3	S, $SmAlO_3$	S, $SmAlO_3$	S, $SmAlO_3$
RF-S3	S, MgO and $SmAlO_3$	S, $SmAlO_3$	S, $SmAlO_3$
AL-S4	S, $SmAlO_3$	S, $SmAlO_3$	S, $SmAlO_3$
AF-S4	S, MgO and $SmAlO_3$	S, $SmAlO_3$	S, $SmAlO_3$
CL-S4	S, $SmAlO_3$	S, $SmAlO_3$	S, $SmAlO_3$
CF-S4	S, MgO and $SmAlO_3$	S, $SmAlO_3$	S, $SmAlO_3$
RL-S4	S, $SmAlO_3$	S, $SmAlO_3$	S, $SmAlO_3$
RF-S4	S, MgO and $SmAlO_3$	S, $SmAlO_3$	S, $SmAlO_3$

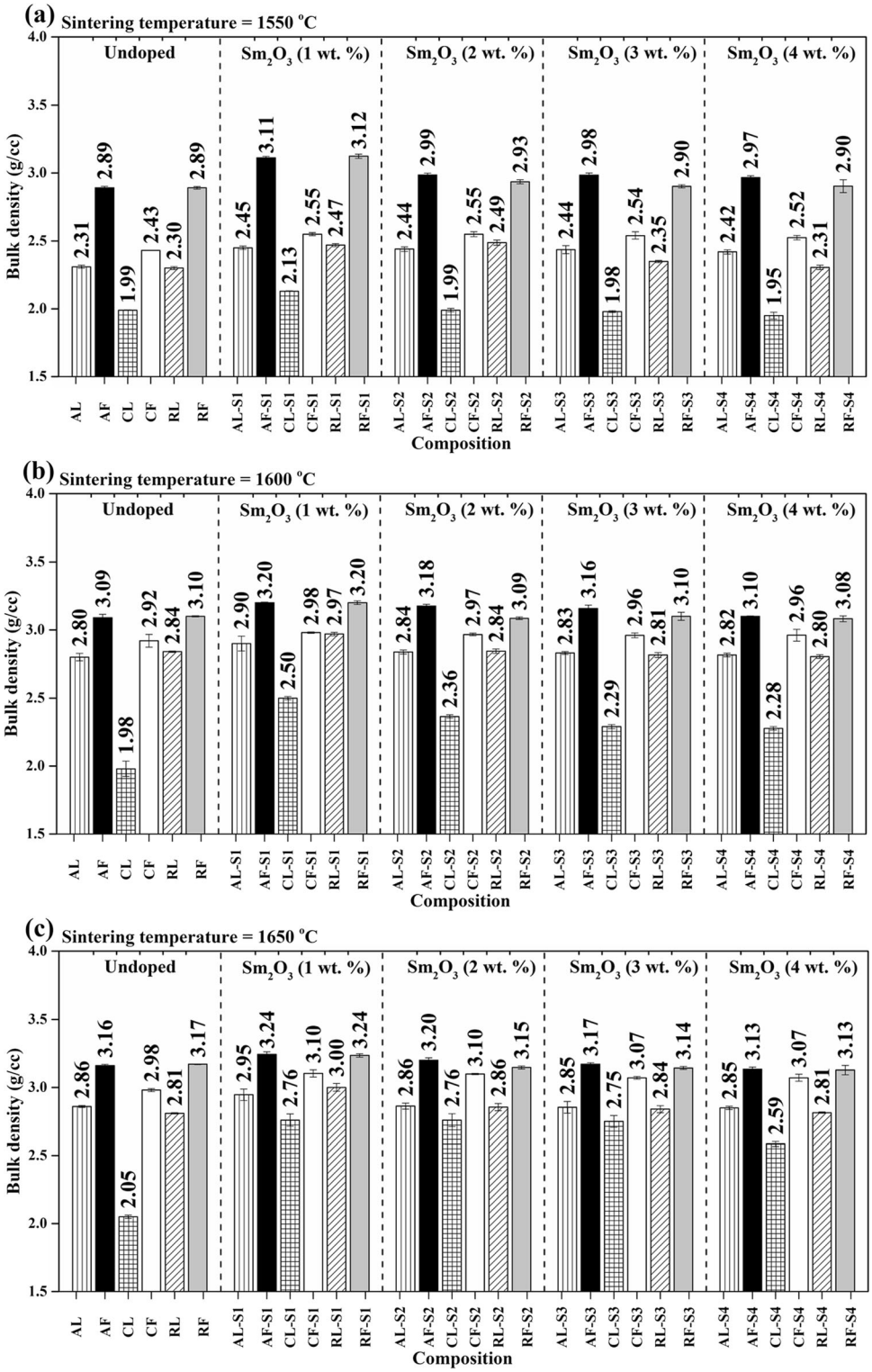

Fig. 3 Bulk densities of the different spinel batches (without additive and Sm_2O_3 doped) fired at (a) 1550 °C, (b) 1600 °C and (c) 1650 °C

sponding elemental analyses are illustrated in Fig. 6. In the current investigation, only a small number of samples were chosen for elemental analyses due to the large number of spinel batches. From the batches that did not contain any additives, AL and CL were chosen to serve as representative samples, whereas the spinel compositions—AF-S1, CL-S1, and RF-S1—were chosen as representative samples among the 1 wt.% samaria-doped specimens. Microstructures and the corresponding EDS spectrums of AL and CL indicate that the grains are largely spinel grains (S) indicated by the presence of elements Al, Mg, and O.

Samarium-rich phases can be identified by their white color and the presence of the elements like Al, Mg, O and Sm, as seen in spots C, D, and E of the fractographs of AF- S1, CL-S1,

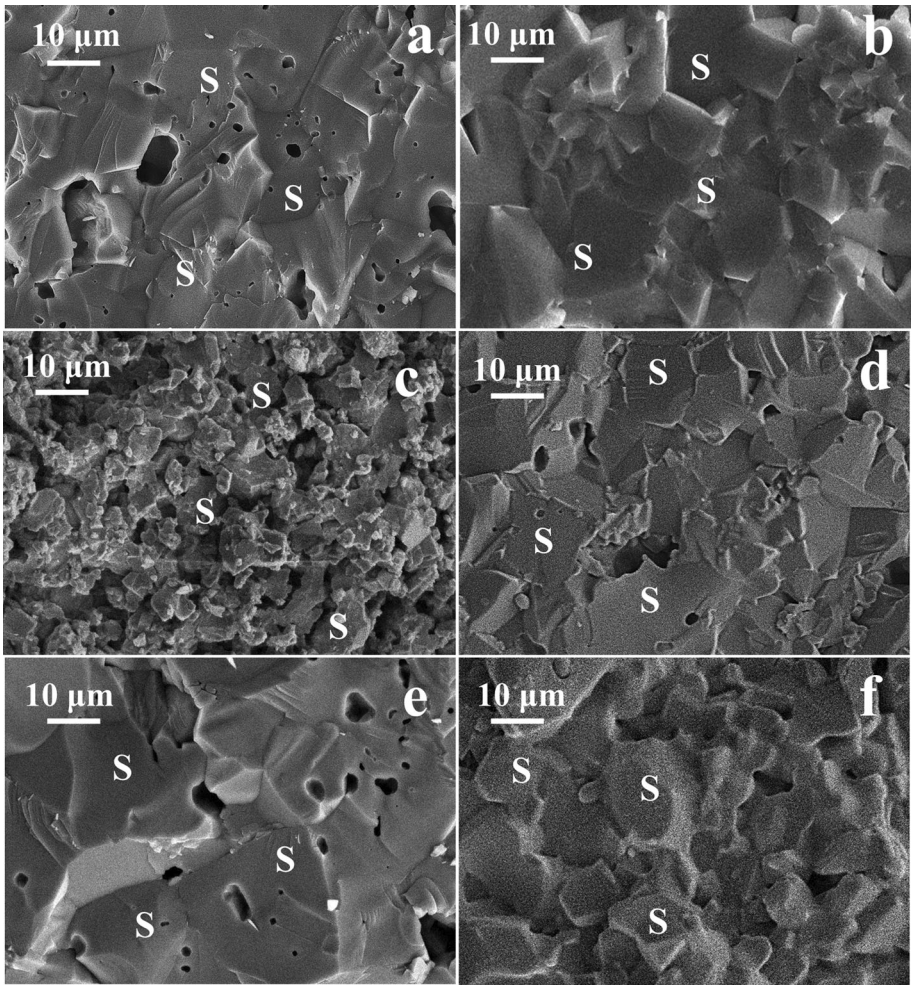

Fig. 4 Fractographs of mixed oxide spinel batches without additive fired at 1650 °C (a) AL (b) AF (c) CL (d) CF (e) RL and (f) RF. (S represents spinel grains.)

and RF-S1, respectively. The gold coating applied to the fractured samples before the microstructural analysis is realized by the peaks in all of the EDS spectra at a voltage of ~ 2.1 keV (Fig. 6).

The following observations may be drawn from the preceding microstructural, density and phase studies. There are two possible explanations why the addition of samaria resulted in density improvement. One, *in situ* generated $SmAlO_3$ and the spinel matrix have a very similar crystal structural arrangement (Ref 46). Furthermore, it is possible that the secondary phase developed separately from the Mag-Al spinel phase due to direct interaction between Sm_2O_3 and Al_2O_3 particles in the mixed powders during sintering. X-ray diffraction analyses reveal that samaria do not enter the spinel structure but forms a separate and distinct compound with alumina ($SmAlO_3$). This $SmAlO_3$ exists as a secondary intergranular phase, mostly along the spinel grain boundaries. To put it another way, the $SmAlO_3$ phase has a ''pinning'' effect on the spinel grains, preventing them from enlarging. In spinel, this samarium-rich phase was found in various pockets at multi-grain junctions. A possible result of this could be improved mechanical properties (Ref 48).

3.5 Mechanical Properties

The above studies suggest that 1 wt.% of Sm_2O_3 was the optimal quantity of additive in the current study. For this reason, both additive-free (0 wt.%) and Sm_2O_3-doped (1 wt.%) spinel batches sintered at 1650 °C were subjected to a series of bulk property tests, including cold strength test (3-point bending strength test carried out at ambient temperature) and estimation of residual strength after thermal shock treatment.

3.5.1 Cold Modulus of Rupture (CMOR). The addition of 1 wt.% Sm_2O_3 clearly improves the CMOR (flexural strength) values of the undoped spinel batches (Fig. 7). The microstructural alteration brought about by the inclusion of Sm_2O_3 and the formation of a secondary phase, samarium aluminate, improved the densification and resulted in a rather uniform grain structure as a result of pinning effect. This controlled microstructure with relatively smaller grains in the samaria-doped spinel batches (as observed from Fig. 4 and 5) led to improved flexural strength than the additive-free spinel batches (Ref 49, 50). According to Quan et al. (Ref 41), samarium aluminate ($SmAlO_3$) may improve mechanical characteristics by stabilizing grain boundaries and limiting the movement of spinel grain boundaries (Ref 41). Some other reports are also available on the literature on the mechanical

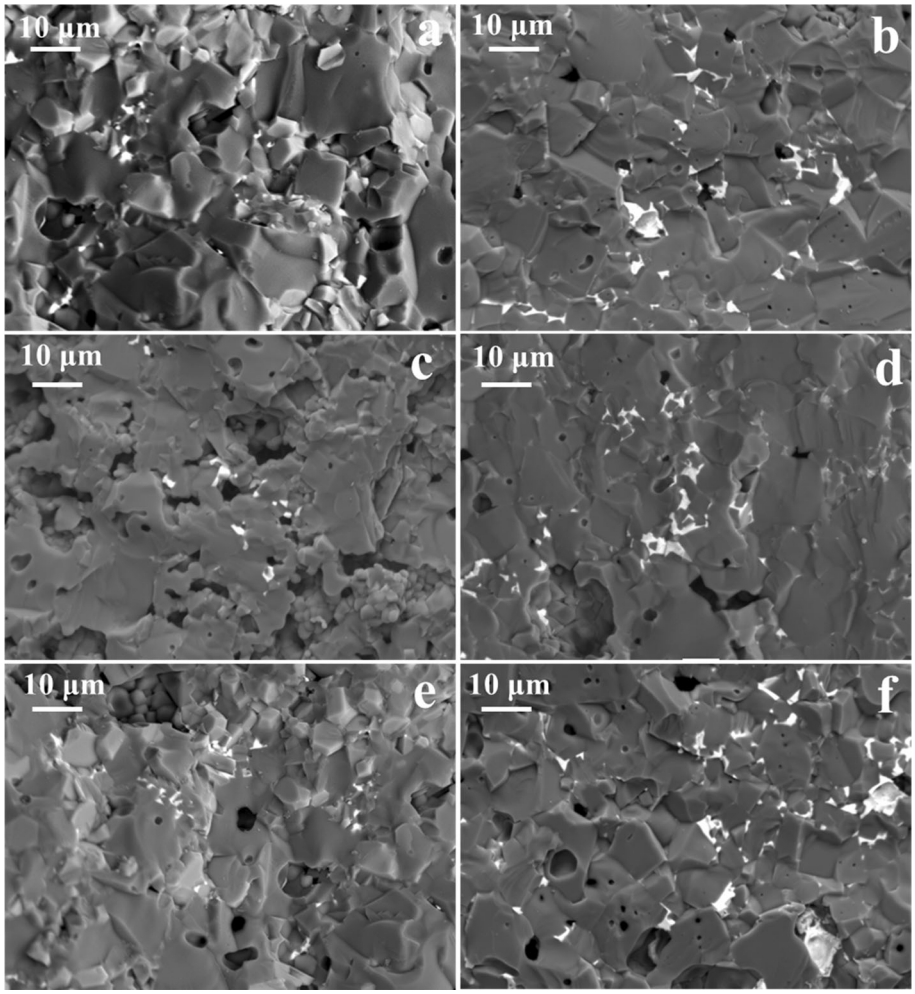

Fig. 5 SEM fractographs (back-scattered mode) of 1 wt.% Sm_2O_3-doped spinel batches sintered at 1650 °C (a) AL-S1 (b) AF-S1 (c) CL-S1 (d) CF-S1 (e) RL-S1 and (f) RF-S1

characterization of samarium aluminate (Ref 51, 52).

3.5.2 Thermal Shock Behavior. Spinel refractories often experience thermal fatigue during service conditions. They undergo a number of thermal cycles leading to stress build-up in the material which then finally leads to failure. Quenching into a liquid medium such as water often introduces a large thermal gradient in the test specimens as opposed to air-quenching. Since the specific heat of water is greater than the specific heat of air, water as a quenching medium has the capability to induce more severe thermal shocks in the test specimens and its effects may be realized with even with fewer number of quench cycles. In the present study, water was used as the quenching medium. After undergoing thermal shock treatment, the absolute (in MPa) and percent strength retainment values of spinel batches (additive-free and samarium oxide (1 wt.%)-doped spinel batches) are illustrated in Fig. 8(a) and (b), respectively, plotted in relation with the number of quench cycles (maximum of 8 thermal cycles). For simplicity, the values of retained strength for additive-free (undoped) compositions are connected with dotted lines, and for batches doped with 1 wt.% Sm_2O_3 with solid lines.

As can be seen in Fig. 8(a) and (b), the addition of samaria improves the strength retention capacity. Even after two heat cycles, the residual strength of the additive-free samples was very low, and there was a significant decrease in retained strength values across all spinel batches. All batches experienced strength deterioration even when samaria was present; however, the decline was greatly mitigated, leading to improved strength retention.

One possible explanation for this enhancement is that the development of $SmAlO_3$, with similar crystal structure to spinel and presence of $SmAlO_3$ at the grain junctions restricting growth, leads to better sintering, which in turn improves densification and strength by acting as a barrier to the propagation of cracks. Better strength retention capability has also come from the presence of the samarium aluminate phase at intergranular sites, which has limited crack migration caused

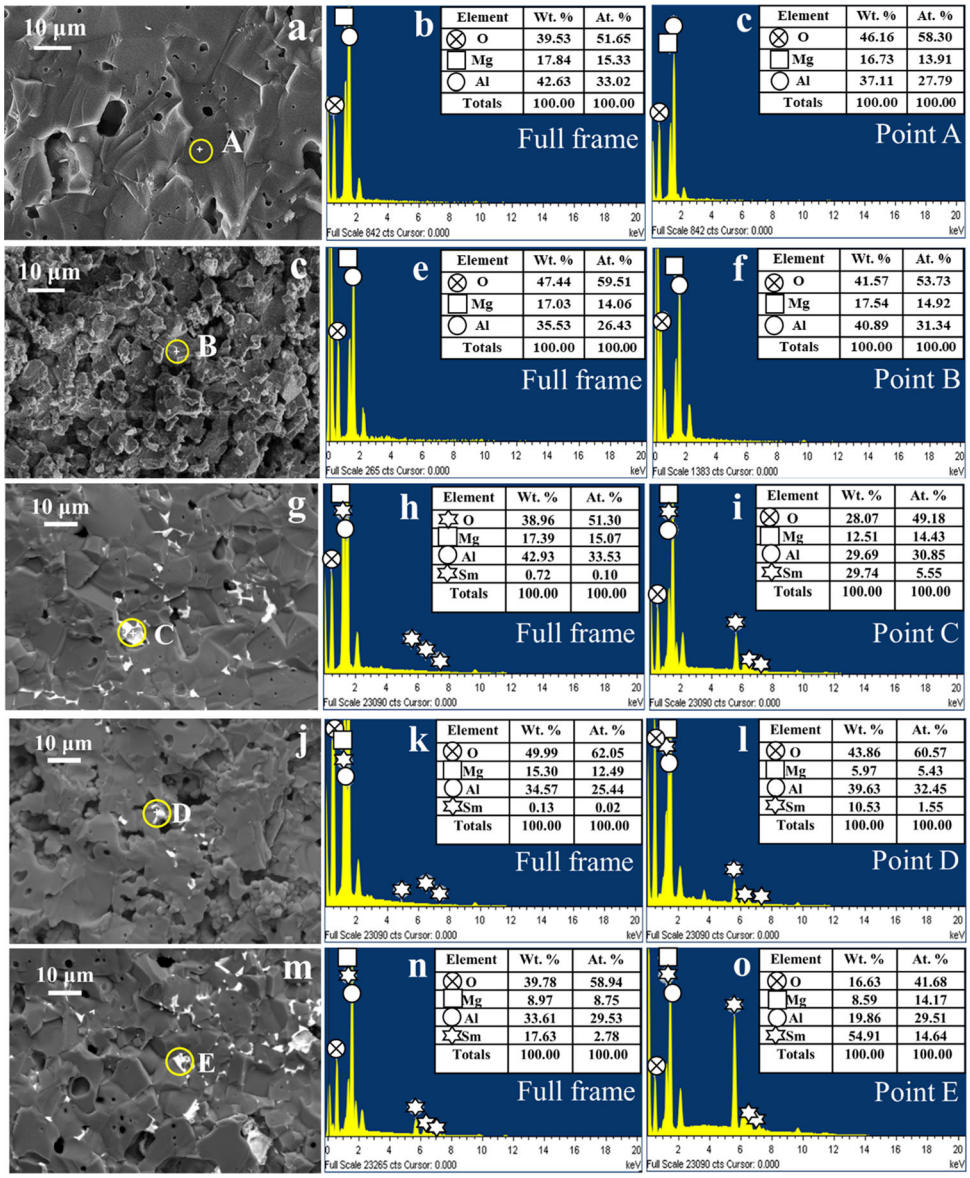

Fig. 6 Complete frame and point elemental analysis of spinel batches fired at 1650.°C. (a) AL (b) Complete frame EDS of AL, (c) Point EDS analysis of AL (Point A). (d) CL (e) Complete frame EDS analysis of CL, (f) Point EDS analysis of CL (Point B). (g) AF-S1 (h) Complete frame EDS analysis of AF-S1, (i) Point EDS analysis of AF-S1 (Point C). (j) CL-S1 (k) Complete frame EDS analysis of CL-S1, (l) Point EDS analysis of CL-S1 (Point D). (m) RF-S1 (n) Complete frame EDS analysis of RF-S1, (o) Point EDS analysis of RF-S1 (Point E)

by thermal stress. The $SmAlO_3$ phase may have contributed to the enhanced thermal shock resistance by delaying the failure of the samples significantly. The $SmAlO_3$ phase helps make this possible by partially filling pores and stabilizing the spinel grain boundaries. The higher densification and strength of the samaria-doped spinel batches has led to improved thermal shock resistance and a better strength-retaining capacity (Ref 42, 53).

All spinel batches follow a similar pattern of decreasing strength retention. Overall, CL had the lowest strength retention capacity of all spinel batches tested, regardless of whether or not the batch included samaria. After 8 heat cycles, CL maintained a retained strength of 6.1 MPa, or 18.2%, but in the presence of samaria (CL-S1), this value increased to 28.13%. The low density and CMOR value of CL batch may account for its poor strength retention capacity. The strength of all the other spinel batches doped with samaria even after 8 quench cycles

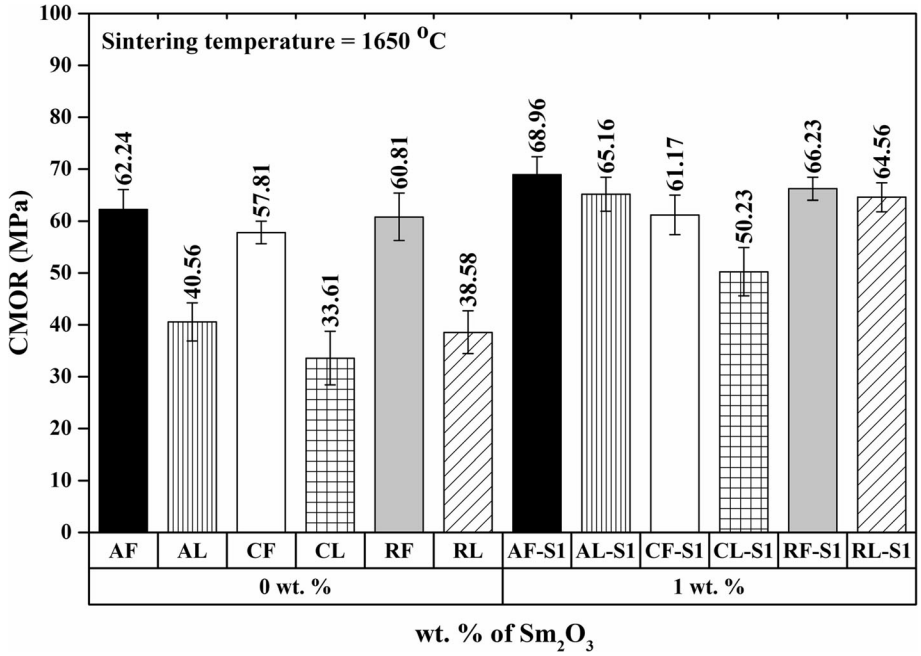

Fig. 7 Flexural strengths of the different spinel compositions (additive-free and 1 wt.% Sm_2O_3 containing) sintered at 1650 °C

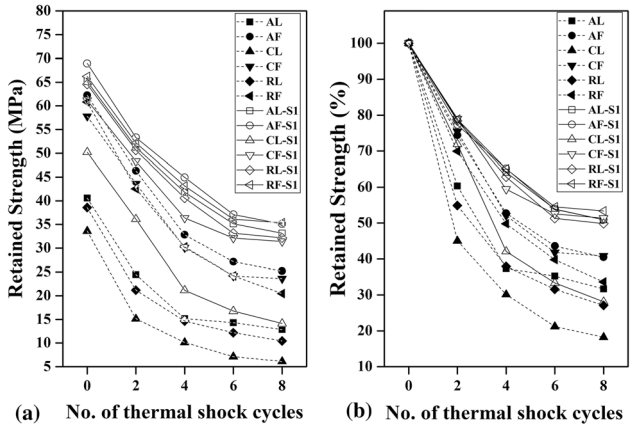

Fig. 8 Variation of residual strength with the no. of thermal (quench) cycles (a) in MPa (b) in %

was between 50 and 53%. Furthermore, for all the additive-containing spinel batches, the drop in retained strength values was much minimized after 4 or 6 quench cycles.

3.6 Thermal Expansion Study

The previous sections on density, strength and thermal shock studies elucidate that batch AF-S1 gave the optimum results, and therefore, the thermal expansion study of batch AF-S1 and its corresponding additive-free batch (AF) is discussed in the current section. Figure 9(a) represents the dimensional changes of the additive-free (AF) and samaria containing (AF-S1) batches with respect to temperature, while Fig. 9(b) represents their corresponding shrinkage rates (in $^{o}C^{-1}$). The composition AF showed expansion (0.98%) up to 1243 °C, while the Sm_2O_3 containing sample AF-S1 showed expansion (0.91%) up to 1155 °C. This similar expansion behavior is quite obvious in both the cases, and this behavior may be attributed to the formation of magnesium aluminate spinel from the constituent oxides since the ratio of MgO: Al_2O_3 was fixed (1:1) in both the compositions. Further, the dimensional changes (shrinkage) associated with samaria containing batch AF-S1 were more than that of AF at 1500 °C due to better sintering (Fig. 9a).

The plot of shrinkage rate versus temperature (Fig. 9b) may be divided into two regimes. The first regime refers to the region where shrinkage rate is positive and is called the *expansion zone*, while the second regime where the shrinkage rate is negative or sintering process is dominant is called the *contraction zone*. The sintering process and the formation of spinel are both thermally activated solid state processes, but occur at different temperatures. Spinel formation begins at a relatively low temperature, while the process of sintering does not begin until much higher temperatures are reached. As a result, the shrinkage caused by the densification of the ceramic at higher temperatures compensates for the initial expansion caused by spinel formation. It is evident that addition of samarium oxide has lowered the temperature at which shrinkage begins (1155 °C) as compared to the additive-free batch (1243 °C). Incorporation of Sm_2O_3 into spinel composition accelerated the densification process, which becomes dominating above 1155 °C. In other words, samaria promoted early sintering by 88 °C in the AF system. Further, the additive-free batch could reach a maximum shrinkage rate of 1.5×10^{-4} °C^{-1} while the samaria containing composition showed a higher shrinkage rate of 2.38×10^{-4} °C^{-1} at 1500 °C.

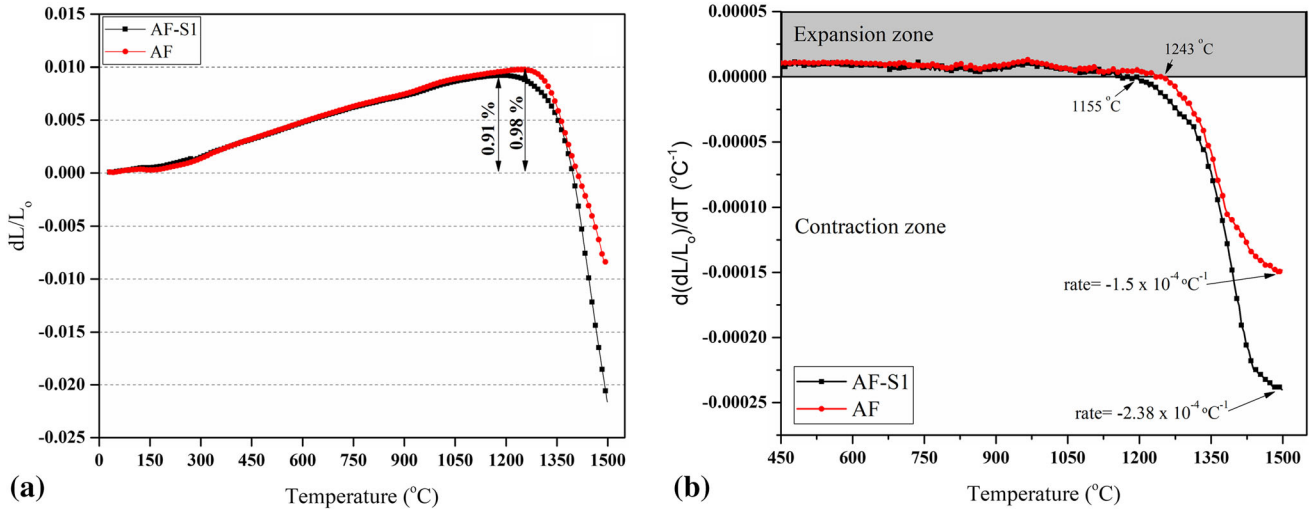

Fig. 9 Dimensional changes associated with AF and AF-S1 with respect to temperature. (b) Shrinkage rate plot for AF and AF-S1 showing the expansion and contraction regimes

4. Conclusions

The current study examines the effect of Sm_2O_3 addition, in concentrations ranging from 1 to 4% by weight, on the density, phase formation and mechanical characteristics of various spinel batches prepared from various commercially available raw materials. The key takeaways from the present study are as follows:

1. Spinel batches with magnesia light had lower density values than those with fused magnesia at all sintering temperatures (1550-1650 °C).
2. Spinel bodies containing Al_2O_3-C had lower density values across all spinel batches, in both additive-free and Sm_2O_3-doped conditions, compared to those containing Al_2O_3-A or Al_2O_3-R, the latter two of which had finer alumina particle sizes.
3. Spinel batches doped with 1 wt.% Sm_2O_3 had improved density and a more controlled grain structure due to the formation $SmAlO_3$ secondary phase with a similar crystal structure arrangement as spinel (cubic).
4. The spinel compositions doped with 1 wt.% Sm_2O_3 outperformed their undoped counterparts in cold-strength as well as residual strength after thermal shock treatment. Due the development of $SmAlO_3$, spinel grain boundaries were stabilized, resulting in increased densification and strength and enhanced thermal shock behavior.

Acknowledgments

The authors would like to offer their sincerest gratitude to Almatis, India, for providing a variety of essential raw materials. Additionally, they would like to express their appreciation to the technical personnel of the Department of Ceramic Engineering, National Institute of Technology, Rourkela, for their timely assistance throughout the course of experiments.

References

1. I. Ganesh, A Review on Magnesium Aluminate ($MgAl_2O_4$) Spinel: Synthesis, Processing and Applications, *Int. Mater. Rev.*, 2013, **58**(2), p 63–112
2. R. Sarkar, Refractory Applications of Magnesium Aluminate Spinel, *Refract. Manual-Interceram*, 2010, p 11–14
3. X. Ren, B. Ma, G. Zhang, G. Fu, J. Yu, and G. Liu, Preparation and Properties of $MgAl_2O_4$ Spinel Ceramics by Double-Doped Sm_2O_3–(Y_2O_3, Nb_2O_5 and La_2O_3), *Mater. Chem. Phys.*, 2020, **252**, p 123309
4. K.E. Sickafus, J.M. Wills, and N.W. Grimes, Structure of Spinel, *J. Amer. Ceram. Soc.*, 1999, **82**(12), p 3279–3292
5. L. Esposito, A. Piancastelli, and S. Martelli, Production and Characterization of Transparent $MgAl_2O_4$ Prepared by Hot Pressing, *J. Eur. Ceram. Soc.*, 2013, **33**(4), p 737–747
6. K. Morita, B.N. Kim, H. Yoshida, and K. Hiraga, Densification Behavior of a fine-Grained $MgAl_2O_4$ Spinel during Spark Plasma Sintering (SPS), *Scr. Mater.*, 2010, **63**(6), p 565–568
7. M. Sokol, M. Halabi, S. Kalabukhov, and N. Frage, Nano-Structured $MgAl_2O_4$ Spinel Consolidated by High Pressure Spark Plasma Sintering (HPSPS), *J. Eur. Ceram. Soc.*, 2017, **37**(2), p 755–762
8. Y. Wen, X. Liu, X. Chen, Q. Jia, R. Yu, and T. Ma, Effect of Heat Treatment Conditions on the Growth of $MgAl_2O_4$ Nanoparticles Obtained by Sol-Gel Method, *Ceram. Int.*, 2017, **43**(17), p 15246–15253
9. D. Ding, L. Lv, G. Xiao, Y. Ren, S. Yang, P. Yang, and X. Hou, One-Step Synthesis of In-Situ Multilayer Graphene Containing $MgAl_2O_4$ Spinel Composite Powders, *Ceram. Int.*, 2019, **45**(5), p 6209–6215
10. K. Mackenzie, J. Temuujin, T. Jadambaa, M. Smith, and P. Angerer, Mechanochemical Synthesis and Sintering Behaviour of Magnesium Aluminate Spinel, *J. Mater. Sci.*, 2000, **35**(22), p 5529–5535
11. S. Takahashi, A. Kan, and H. Ogawa, Microwave Dielectric Properties and Crystal Structures of Spinel-Structured $MgAl_2O_4$ Ceramics Synthesized by a Molten-Salt Method, *J. Eur. Ceram. Soc.*, 2017, **37**(3), p 1001–1006
12. A. Zegadi, M. Kolli, M. Hamidouche, and G. Fantozzi, Transparent $MgAl_2O_4$ Spinel Fabricated by Spark Plasma Sintering from Commercial Powders, *Ceram. Int.*, 2018, **44**(15), p 18828–18835
13. L.L. Zhu, Y.J. Park, L. Gan, S.I. Go, H.N. Kim, J.M. Kim, and J.W. Ko, Fabrication of Transparent $MgAl_2O_4$ from Commercial Nanopowders by Hot-Pressing Without Sintering Additive, *Mater. Lett.*, 2018, **219**, p 8–11
14. M.T. Camargo, Q. Jacques, L.B. Caliman, J. Miagava, D. Hotza, R.H. Castro, and D. Gouvêa, Synthesis of Ca-Doped Spinel by Ultrasonic Spray Pyrolysis, *Mater. Lett.*, 2016, **171**, p 232–235

15. L. Yuan, B. Ma, Q. Zhu, Z. Wang, G. Li, and J. Yu, Preparation and Properties of $MgAl_2O_4$ Based Ceramics Reinforced With Rod-Like Microcrystallines by Co-Doping Sm_2O_3 and La_2O_3, *Ceram. Int.*, 2017, **43**(18), p 16258–16263
16. R. Sarkar and S. Sahoo, Effect of Raw Materials on Formation and Densification of Magnesium Aluminate Spinel, *Ceram. Int.*, 2014, **40**(10), p 16719–16725
17. S. Sinhamahapatra, C. Ghosh, H.S. Tripathi, and S. Mukhopadhyay, Effect of Yb_2O_3 and TiO_2 on Reaction Sintering and Properties of Magnesium Aluminate Spinel, *Ceram. Int.*, 2021, **47**(19), p 27372–27385
18. S.K. Mohan and R. Sarkar, A Comparative Study on the Effect of Different Additives on the Formation and Densification of Magnesium Aluminate Spinel, *Ceram. Int.*, 2016, **42**(12), p 13932–13943
19. I. Ganesh, S.M. Olhero, A.H. Rebelo, and J.M. Ferreira, Formation and Densification Behavior of $MgAl_2O_4$ Spinel: The Influence of Processing Parameters, *J. Amer. Ceram. Soc.*, 2008, **91**(6), p 1905–1911
20. R. Sarkar, S.K. Das, and G. Banerjee, Effect of Attritor Milling on the Densification of Magnesium Aluminate Spinel, *Ceram. Int.*, 1999, **25**(5), p 485–489
21. R. Sarkar and G. Banerjee, Effect of Compositional Variation and Fineness on the Densification of $MgO–Al_2O_3$ Compacts, *J. Eur. Ceram. Soc.*, 1999, **19**(16), p 2893–2899
22. C.J. Ting and H.Y. Lu, Defect Reactions and the Controlling Mechanism in the Sintering of Magnesium Aluminate Spinel, *J. Amer. Ceram. Soc.*, 1999, **82**(4), p 841–848
23. P. Ugur and C. Aksel, The Effect of SnO_2 on the Improvement of Mechanical Properties of $MgO–MgAl_2O_4$ Composites, *Compos. B Eng.*, 2012, **43**(5), p 2217–2221
24. R. Naghizadeh, H. Rezaie, and F. Golestani-Fard, Effect of TiO_2 on Phase Evolution and Microstructure of $MgAl_2O_4$ Spinel in Different Atmospheres, *Ceram. Int.*, 2011, **37**(1), p 349–354
25. R. Sarkar and G. Bannerjee, Effect of Addition of TiO_2 on Reaction Sintered $MgO–Al_2O_3$ Spinels, *J. Eur. Ceram. Soc.*, 2000, **20**(12), p 2133–2141
26. S. Sinhamahapatra, K. Dana, A. Ghosh, V.P. Reddy, and H.S. Tripathi, Dynamic Thermal Study to Rationalise the Role of Titania in Reaction Sintering of Magnesia-Alumina System, *Ceram. Int.*, 2015, **41**(1), p 1073–1078
27. S. Sinhamahapatra, K. Dana, and H.S. Tripathi, Enhancement of Reaction-Sintering of Alumina-Excess Magnesium Aluminate Spinel in Presence of Titania, *Ceram. Int.*, 2018, **44**(9), p 10773–10780
28. R. Sarkar, S.K. Das, and G. Banerjee, Effect of Addition of Cr_2O_3 on the Properties of Reaction Sintered $MgO–Al_2O_3$ Spinels, *J. Eur. Ceram. Soc.*, 2002, **22**(8), p 1243–1250
29. A. Ghosh, S. Das, J. Biswas, H.S. Tripathi, and G. Banerjee, The Effect of ZnO Addition on the Densification and Properties of Magnesium Aluminate Spinel, *Ceram. Int.*, 2000, **26**(6), p 605–608
30. E. Kostić, S. Bošković, and Š Kiš, Influence of Fluorine Ion on the Spinel Synthesis, *J. Mater. Sci. Lett.*, 1982, **1**(12), p 507–510
31. J.L. Huang, S.Y. Sun, and Y.C. Ko, Investigation of High-Alumina Spinel: Effect of LiF and $CaCO_3$ Addition, *J. Amer. Ceram. Soc.*, 1997, **80**(12), p 3237–3241
32. S.K. Chen, M.Y. Cheng, and S.J. Lin, Reducing the Sintering Temperature for $MgO–Al_2O_3$ Mixtures by Addition of Cryolite (Na_3AlF_6), *J. Amer. Ceram. Soc.*, 2002, **85**(3), p 540–544
33. R. Lodha, A. Ghosh, B. Mukherjee, and G. N. Agrawal, Zirconia-magnesium aluminate spinel composite-Improved ZrO_2-$MgAl_2O_4$ composite was prepared by solid-state sintering, *Amer. Ceram. Soc. Bull.*, 2006, **85**(6)
34. I. Ganesh, S. Bhattacharjee, B.P. Saha, R. Johnson, and Y.R. Mahajan, A New Sintering aid for Magnesium Aluminate Spinel, *Ceram. Int.*, 2001, **27**(7), p 773–779
35. S.K. Mohan and R. Sarkar, Effect of ZrO_2 Addition on $MgAl_2O_4$ Spinel from Commercial Grade Oxide Reactants, *Ceram. Int.*, 2016, **42**(8), p 10355–10365
36. S.K. Mohan and R. Sarkar, Reaction Sintered Zinc Oxide Incorporated Magnesium Aluminate Spinel from Commercial Grade Oxide Reactants, *J. Aust. Ceram. Soc.*, 2017, **53**(1), p 207–216
37. R. Sarkar, S.K. Das, and G. Banerjee, Effect of Additives on the Densification of Reaction Sintered and Presynthesised Spinels, *Ceram. Int.*, 2003, **29**(1), p 55–59
38. Z. Quan, Z. Wang, X. Wang, H. Liu, and Y. Ma, Effect of CeO_2 Addition on the Sintering Behavior of Pre-Synthesized Magnesium Aluminate Spinel Ceramic Powders, *Ceram. Int.*, 2019, **45**(1), p 488–493
39. B. Baruah and R. Sarkar, Rare-Earth Oxide-Doped Magnesium Aluminate Spinel - An Overview, *Interceram Int. Ceram. Rev.*, 2020, **69**(3), p 40–45
40. B. Ma, Y. Yin, Q. Zhu, Y. Li, G. Li, and J. Yu, In-Situ Formation and Densification of $MgAl_2O_4$-$SmAlO_3$ Ceramics by a Single-Stage Reaction Sintering Process, *Ceram. Silik.*, 2015, **59**(2), p 109–114
41. Z. Quan, Z. Wang, X. Wang, H. Liu, and Y. Ma, Effects of Sm_2O_3 Addition on Sintering Behavior of Pre-Synthesized Magnesia-Rich Magnesium Aluminate Spinel, *J. Rare Earths*, 2021, **39**(11), p 1450–1454
42. B. Baruah and R. Sarkar, Effect of Y_2O_3 Content on Densification, Microstructure and Mechanical Properties of Reaction Sintered Magnesium Aluminate Spinel, *Ceram. Int.*, 2023, **49**(1), p 755–765
43. S. Sinhamahapatra, K. Dana, S. Mukhopadhyay, and H.S. Tripathi, Role of Different Rare Earth Oxides on the Reaction Sintering of Magnesium Aluminate Spinel, *Ceram. Int.*, 2019, **45**(9), p 11413–11420
44. M.N. Rahaman, *Ceramic Processing*, CRC Press, Boca Raton, 2017
45. R. Sarkar, H.S. Tripathi, and A. Ghosh, Reaction Sintering of Different Spinel Compositions in the Presence of Y_2O_3, *Mater. Lett.*, 2004, **58**(16), p 2186–2191
46. J. Liu, Z. Wang, H. Liu, X. Wang, and Y. Ma, Effect of Y_2O_3 Doping on the High-Temperature Properties of Magnesia Aluminate Spinel Refractories, *J. Aust. Ceram. Soc.*, 2020, **56**(2), p 389–394
47. S. Lakiza and L. Lopato, Phase Diagram of the Alumina–Zirconia–Samaria System, *J. Amer. Ceram. Soc.*, 2006, **89**(11), p 3516–3521
48. Y. Yijun and Q. Tai, Effect of Y_2O_3 and Dy_2O_3 on Microstructure and Mechanical Behaviors of Aluminum Nitride Ceramics, *J. Rare Earths*, 2006, **24**(1), p 239–243
49. J. Liu, X. Lv, J. Li, and L. Jiang, Pressureless Sintered Magnesium Aluminate Spinel with Enhanced Mechanical Properties Obtained by the Two-Step Sintering Method, *J. Alloys Compd.*, 2016, **680**, p 133–138
50. J. Liu, X. Lv, J. Li, L. Zhang, and J. Peng, Densification and Microstructure of Magnesium Aluminate Spinel for Adding Method of Sc_2O_3, *J. Alloys Compd.*, 2018, **735**, p 394–399
51. K.K. Bamzai, V. Singh, P.N. Kotru, and B.M. Wanklyn, Micromechanical Characteristics of Flux-Grown $SmAlO_3$ Single Crystal, *Strength Mater.*, 2010, **42**(4), p 387–396
52. P.N. Kotru, K.K. Raina, S.K. Kachroo, and B.M. Wanklyn, Microhardness Measurements on Single Crystals of Flux-Grown Rare Earth Perovskites (Orthoferrites, Orthochromites and Aluminates), *J. Mater. Sci.*, 1984, **19**(18), p 2582–2592
53. R. Sarkar, *Refractory Technology: Fundamentals and Applications*, CRC Press, Boca Raton, 2016, p 48